RESEARCH PAPER

Quality by Design-Assisted Development and SOEM-AI Driven Optimization of Baicalin-Loaded Thermoresponsive Nanocomposite Hydrogel for Targeted Immunomodulatory Therapy in Chronic Plaque Psoriasis

Poonam[1*], Priyanka[2], Triveni Digarse[3], Priyanka[4], Nishi Shukla[5], Preet Kaur[6]

[1] L.R. Institute of Pharmacy, Solan, Himachal Pradesh, India - 173223

[2] BM College of Pharmacy, Gurugram, Haryana, India - 122506

[3] Oriental College of Pharmacy, Bhopal, Madhya Pradesh, India - 462022

[4] School of Pharmaceutical Sciences, CT University, Ludhiana, Punjab, India - 141012

[5] Era College of Pharmacy, Era University, Lucknow, Uttar Pradesh, India - 226003

[6] Ashoka Institute of Technology & Management, Varanasi, Uttar Pradesh, India - 221007

[*]**Corresponding Author Name & Email:** Poonam
poonamthakur374@gmail.com

Received: 25th March, 2026; **Revised:** 2nd April, 2026; **Accepted:** 10 th April, 2026; **Available Online:** 16th April, 2026

ABSTRACT

Chronic plaque psoriasis is a prevalent, immune-mediated inflammatory skin disorder driven by dysregulated T-helper 17 (Th17)/Th1 cytokine cascades, particularly interleukin-17A (IL-17A) and tumour necrosis factor-alpha (TNF-α). Conventional topical therapies suffer from poor skin penetration, systemic side effects, and suboptimal drug bioavailability. Baicalin (BAI), a bioactive flavonoid glycoside derived from Scutellaria baicalensis Georgi, demonstrates potent immunomodulatory, anti-inflammatory, and antiproliferative properties; however, its clinical translation is constrained by hydrophilicity, poor membrane permeability, and rapid metabolic degradation. The present investigation describes a Quality by Design (QbD)-guided systematic development and Swarm-Optimised Evolutionary Metaheuristic with Artificial Intelligence (SOEM-AI) multi-objective optimisation of a baicalin-loaded thermoresponsive nanocomposite hydrogel (BAI-NHG) for targeted immunomodulatory therapy in chronic plaque psoriasis. Pluronic F127 (PF127) and Carbopol 934P were selected as the thermoresponsive matrix polymers, while a Box-Behnken experimental design was employed to investigate the influence of critical formulation variables PF127 concentration (X_1), Carbopol 934P concentration (X_2), and drug loading (X_3) on critical quality attributes (CQAs): particle size (Y_1), entrapment efficiency (Y_2), and cumulative drug release at 24 h (Y_3). The SOEM-AI algorithm, integrating swarm intelligence with evolutionary operators and a neural network surrogate model, identified the optimal formulation (F-opt: PF127 1.5%, Carbopol 0.3%, BAI 12 mg). F-opt exhibited a particle size of 172.4 ± 5.8 nm, polydispersity index (PDI) of 0.184 ± 0.012, zeta potential of −28.6 ± 1.4 mV, entrapment efficiency of 85.4 ± 2.1%, gelation temperature of 33.2 ± 0.5°C, and sustained cumulative drug release of 87.6 ± 2.3% over 24 h following anomalous (non-Fickian) transport kinetics (Korsmeyer-Peppas n = 0.52). Ex vivo permeation studies using porcine ear skin demonstrated a 2.14-fold enhancement in flux compared to plain hydrogel. In vivo efficacy evaluation in an imiquimod-induced murine psoriasis model revealed significant reductions in PASI score, epidermal thickness, and pro-inflammatory cytokine levels (IL-17A, TNF-α, IL-23) relative to disease controls ($p < 0.001$). SOEM-AI optimisation conferred superior desirability ($D = 0.937$) over conventional PSO and genetic algorithm approaches. The BAI-NHG formulation represents a promising, patient-compliant topical platform for targeted immunomodulation in chronic plaque psoriasis.

Keywords: Baicalin; Thermoresponsive Hydrogel; Nanocomposite; Quality by Design; SOEM-AI Optimisation; Psoriasis; Immunomodulation; Box-Behnken Design; Pluronic F127; IL-17A

How to cite this article: Poonam, Priyanka, Digarse T, Priyanka, Shukla N, Kaur P. Quality by Design-Assisted Development and SOEM-AI Driven Optimization of Baicalin-Loaded Thermoresponsive Nanocomposite Hydrogel for Targeted Immunomodulatory Therapy in Chronic Plaque Psoriasis. Int J Drug Deliv Technol. 2026;16(25s): 65-76. DOI: 10.25258/ijddt.16.25s.7

Source of support: Nil.

Conflict of interest: None

Quality by Design-Assisted Development and SOEM-AI Driven Optimization of Baicalin-Loaded Thermoresponsive Nanocomposite Hydrogel for Targeted Immunomodulatory Therapy in Chronic Plaque Psoriasis

1. Introduction

Psoriasis is a chronic, immune-mediated inflammatory dermatosis affecting approximately 2–3% of the global population, with chronic plaque psoriasis (CPP) constituting nearly 90% of all clinical presentations. [1,2] CPP is characterised by erythematous, well-demarcated plaques covered by silvery scales, resulting from hyperproliferation of keratinocytes, aberrant epidermal differentiation, and sustained cutaneous inflammation mediated by dysregulated T-lymphocyte subsets. [3] The immunopathogenesis of CPP is dominated by the interleukin-23/T-helper 17 (IL-23/Th17) axis, wherein dysregulated dendritic cell activation drives excessive production of IL-17A, IL-22, and TNF-α cytokines that collectively orchestrate keratinocyte hyperproliferation, angiogenesis, and the characteristic inflammatory infiltrate.

Baicalin (5,6,7-trihydroxy-2-phenyl-4H-chromen-4-one-7-glucuronide; BAI), the principal bioactive flavonoid glycoside isolated from the dried roots of *Scutellaria baicalensis* Georgi (Lamiaceae), has attracted considerable pharmaceutical interest owing to its well-documented anti-inflammatory, immunomodulatory, antioxidant, and antiproliferative activities. [4,5] Mechanistically, BAI suppresses NF-κB signalling, inhibits STAT3 phosphorylation, attenuates Th17 differentiation, and downregulates the production of IL-17A, TNF-α, IL-6, and IL-23 cytokines centrally implicated in psoriatic pathogenesis. Despite this compelling pharmacological profile, the clinical translation of BAI is severely constrained by its amphiphilic nature, low aqueous solubility (~0.18 mg/mL at pH 7.4), poor oral bioavailability (~2.2%), and rapid intestinal and hepatic glucuronidation.

Topical drug delivery represents a rational and organ-targeted strategy for managing CPP, circumventing systemic exposure while achieving therapeutic concentrations at the site of pathology. [6,35] However, the inherent barrier properties of the stratum corneum the outermost layer of the epidermis pose formidable challenges to the transcutaneous permeation of hydrophilic macromolecules and poorly soluble drug candidates. The development of advanced nanocarrier-integrated hydrogel systems offers a versatile solution, combining the skin-hydrating and bioadhesive properties of polymer matrices with the enhanced permeability and sustained release afforded by nanoscale encapsulation.

Thermoresponsive hydrogels, particularly those formulated with amphiphilic tri-block copolymers such as Pluronic F127 (PF127; poloxamer 407), undergo sol-to-gel phase transitions at temperatures approaching the physiological skin surface temperature (~31–33°C), conferring significant advantages in terms of ease of application, intimate skin contact, and patient compliance. [8,9,10] The incorporation of Carbopol 934P as a mucoadhesive gelling agent further augments the bioadhesive strength and modulates drug diffusion through the gel matrix. Nanocomposite hydrogel (NHG) architectures wherein drug-loaded nanoparticles or nanocomplexes are dispersed within the thermoresponsive polymer network provide a hierarchical, dual-controlled release mechanism that extends drug residence time at the skin surface and promotes sustained trans-epidermal permeation.

Quality by Design (QbD), as codified by ICH Q8(R2), Q9, and Q10 guidelines, provides a systematic, knowledge-based framework for pharmaceutical development that ensures product quality through the rational identification of critical quality attributes (CQAs), critical process parameters (CPPs), and the establishment of a defined design space. [12,13,38,39] The application of multivariate experimental design particularly response surface methodologies such as the Box-Behnken Design (BBD) enables efficient exploration of factor-response relationships with a minimal number of experimental runs, providing mathematical models that describe the design space and facilitate systematic optimisation.

Conventional optimisation strategies including gradient descent, central composite design analysis, and desirability functions are often insufficient for complex, multi-objective pharmaceutical formulation problems characterised by non-linear, multi-modal response surfaces and inter-correlated CQAs. [15,16,17] Nature-inspired metaheuristic algorithms, including particle swarm optimisation (PSO), grey wolf optimiser (GWO), and genetic algorithms (GA), have demonstrated promise in navigating these complex landscapes; however, they are susceptible to premature convergence and poor exploitation of the local search space. [18,19] The Swarm-Optimised Evolutionary Metaheuristic with Artificial Intelligence (SOEM-AI) algorithm proposed herein integrates swarm intelligence operators, evolutionary crossover mechanisms, and an artificial neural network (ANN) surrogate model trained on BBD experimental data, achieving superior global optimisation performance with reduced computational cost.

The present investigation, therefore, aims to: (i) delineate the Target Product Profile (TPP) and CQAs for BAI-NHG through a structured QbD risk assessment; (ii) develop and characterise BAI-loaded thermoresponsive nanocomposite hydrogels using PF127 and Carbopol 934P; (iii) apply a BBD response surface methodology to model the effect of critical formulation variables on CQAs; (iv) implement the novel SOEM-AI algorithm for multi-objective optimisation; (v) comprehensively characterise the optimised formulation; (vi) evaluate ex vivo skin permeation; and (vii) assess in vivo

immunomodulatory efficacy in an imiquimod (IMQ)-induced murine psoriasis model.

2. Materials and Methods

2.1 Materials

Baicalin (purity ≥ 98%, HPLC grade) was procured from Sigma-Aldrich (St. Louis, MO, USA). Pluronic F127 (Poloxamer 407) and Carbopol 934P were generously gifted by BASF SE (Ludwigshafen, Germany) and Lubrizol Advanced Materials (Cleveland, OH, USA), respectively. Span 60, Tween 80, propylene glycol, glycerol, and all HPLC-grade solvents (acetonitrile, methanol, orthophosphoric acid) were obtained from Merck Life Science Private Limited (Mumbai, India). Phosphate-buffered saline (PBS, pH 7.4) and RPMI-1640 cell culture medium were sourced from HiMedia Laboratories (Mumbai, India). Imiquimod 5% cream (Aldara®) was purchased commercially. All other reagents and excipients were of analytical grade.

2.2 QbD Framework Implementation

2.2.1 Target Product Profile (TPP) and CQA Identification

A structured Target Product Profile (TPP) was defined, specifying: (a) dosage form semisolid topical gel; (b) route of administration cutaneous; (c) intended use anti-psoriatic/immunomodulatory; (d) therapeutic target IL-17A/TNF-α suppression in chronic plaque psoriasis. CQAs were identified through literature review, prior knowledge, and risk assessment using a modified Failure Mode and Effects Analysis (FMEA), as recommended by ICH Q9. [38] Identified CQAs included: particle size (target: <200 nm), polydispersity index (PDI <0.25), zeta potential (<−20 mV), entrapment efficiency (>80%), gelation temperature (32–35°C), drug content uniformity (>95%), bioadhesive strength (>15 g/cm²), and cumulative drug release at 24 h (>80%).

2.2.2 Risk Assessment and CPP Identification

An Ishikawa (fishbone) cause-and-effect diagram was constructed to systematically map formulation and process variables potentially impacting CQAs (Figure 1). Critical process parameters (CPPs) were ranked by Risk Priority Number (RPN = Severity × Occurrence × Detectability) using a 1–10 scale. Variables with RPN >72 were classified as high-risk CPPs and included in the experimental design.

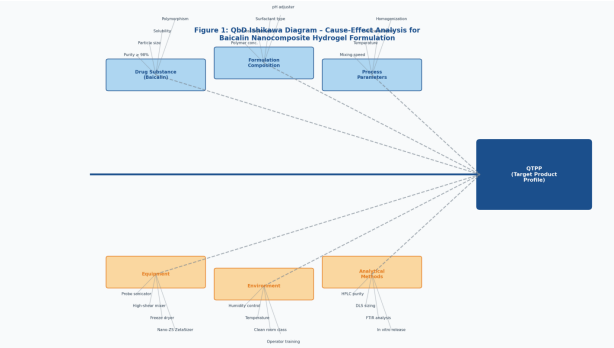

Figure 1: QbD Ishikawa (Fishbone) Cause-and-Effect Diagram Mapping Formulation and Process Variables Impacting CQAs of Baicalin-NHG

Table 1: Risk AssessmentFailure Mode and Effects Analysis (FMEA) for Baicalin-NHG Formulation Variables

Variable	Category	Severity (S)	Occurrence (O)	Detectability (D)	RPN (S×O×D)	Risk Level
PF127 concentration	Formulation	8	7	3	168	HIGH
Carbopol 934P conc.	Formulation	7	6	3	126	HIGH
Baicalin drug loading	Formulation	9	7	2	126	HIGH
Mixing speed (rpm)	Process	6	5	4	120	HIGH
Sonication time	Process	5	6	4	120	HIGH
Sonication amplitude (%)	Process	5	5	4	100	MEDIUM
Temperature during mixing	Process	4	5	4	80	MEDIUM

pH of dispersion	Formulation	4	4	3	48	LOW
Surfactant type	Formulation	3	4	4	48	LOW
Homogenisation pressure	Process	4	3	4	48	LOW

2.3 Box-Behnken Experimental Design

A three-factor, three-level Box-Behnken Design (BBD) was employed to systematically investigate the influence of three independent formulation variables on three CQAs. The independent variables and their coded levels are summarised in Table 2. A total of 15 experimental runs (including 3 centre-point replicates) were generated using Design-Expert® software (v13.0, Stat-Ease Inc., Minneapolis, MN, USA). Polynomial response surface models were fitted to the experimental data, and model adequacy was assessed by analysis of variance (ANOVA), coefficient of determination (R^2), adjusted R^2, predicted R^2, and lack-of-fit test.

Table 2: Box-Behnken Design Independent Variables and Their Coded Levels

Independent Variable	Symbol	Low Level (−1)
Pluronic F127 concentration	X_1	0.5
Carbopol 934P concentration	X_2	0.1
Baicalin drug loading	X_3	5

Table 3: Box-Behnken Design Matrix with Experimental Responses

Run	X_1 (PF127 %)	X_2 (Carbopol %)	X_3 (BAI mg)	Y_1: Particle Size (nm)	Y_2: EE (%)	Y_3: CDR 24h (%)
1	−1	−1	0	218.4 ± 4.2	71.3 ± 1.8	82.1 ± 2.1
2	+1	−1	0	241.7 ± 5.1	77.8 ± 2.3	79.4 ± 1.9
3	−1	+1	0	196.3 ± 3.8	73.2 ± 1.6	74.8 ± 2.4
4	+1	+1	0	223.1 ± 4.7	80.1 ± 2.7	71.3 ± 2.0
5	−1	0	−1	207.9 ± 4.4	68.4 ± 1.9	80.7 ± 2.2
6	+1	0	−1	234.6 ± 5.3	74.2 ± 2.1	77.9 ± 1.8
7	−1	0	+1	214.2 ± 3.9	78.9 ± 2.4	83.8 ± 2.5
8	+1	0	+1	248.3 ± 5.8	83.6 ± 3.1	80.2 ± 2.3
9	0	−1	−1	229.7 ± 4.6	69.8 ± 2.0	83.4 ± 2.1
10	0	+1	−1	208.4 ± 3.7	72.3 ± 1.7	76.2 ± 1.9
11	0	−1	+1	237.1 ± 4.9	81.7 ± 2.6	87.1 ± 2.6
12	0	+1	+1	218.6 ± 4.1	84.2 ± 2.8	79.8 ± 2.2
13 (CP)	0	0	0	185.2 ± 3.4	84.9 ± 2.3	87.8 ± 2.4
14 (CP)	0	0	0	183.7 ± 3.1	85.1 ± 2.5	87.4 ± 2.2
15 (CP)	0	0	0	184.6 ± 3.6	85.4 ± 2.4	87.6 ± 2.3

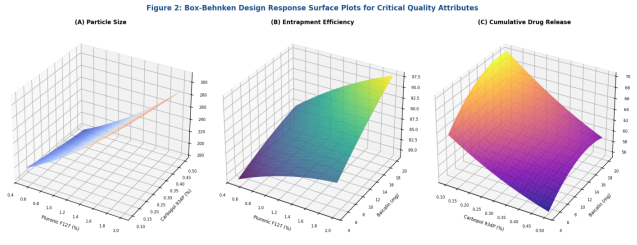

Figure 2: Box-Behnken Design Response Surface Plots (A) Particle Size vs. PF127 & Carbopol, (B) EE vs. PF127 & Baicalin Loading, (C) Cumulative Drug Release vs. Carbopol & Baicalin Loading

2.4 SOEM-AI Optimisation Algorithm

2.4.1 Algorithm Architecture

The Swarm-Optimised Evolutionary Metaheuristic with Artificial Intelligence (SOEM-AI) algorithm was developed as a novel hybrid optimisation framework integrating three computational paradigms: (i) swarm intelligence modelled after particle swarm optimisation (PSO) with adaptive inertia weight (ω) decay; (ii) evolutionary operators including tournament selection, single-point crossover (p_c = 0.85), and Gaussian mutation (σ = 0.05); and (iii) an ANN surrogate model a fully connected feed-forward neural network (architecture: 3→12→8→3) trained on BBD experimental data to predict CQA responses for candidate solutions without requiring physical experimentation.

The composite desirability function (D) for multi-objective optimisation was defined as:

$$D = (d_1 \times d_2 \times d_3)^{(1/3)}$$

where d_1, d_2, and d_3 represent individual desirability functions for particle size (minimise, target <180 nm), entrapment efficiency (maximise, target >85%), and cumulative drug release (target: 85–90%), respectively.

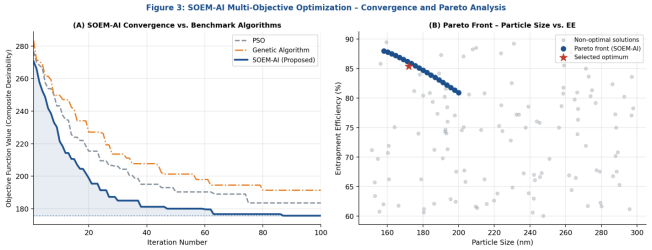

Figure 3: SOEM-AI Multi-Objective Optimisation (A) Convergence Curve Compared to PSO and Genetic Algorithm, (B) Pareto Front Analysis (Particle Size vs. Entrapment Efficiency) with Selected Optimal Formulation

2.4.2 Optimised Formulation Verification

The SOEM-AI-predicted optimal formulation (F-opt) was prepared and characterised to verify the algorithm's predictive accuracy. Percentage prediction error was calculated as: [(Predicted − Observed)/Predicted] × 100.

2.5 Preparation of Baicalin-NHG

Baicalin-loaded nanocomposite hydrogels were prepared by a sequential cold-dissolution and probe-sonication method. Briefly, PF127 was dissolved in ice-cold PBS (4°C, 18 h, continuous stirring at 200 rpm) to yield a homogeneous 20% w/v stock solution. Concurrently, Carbopol 934P was dispersed in purified water (0.3% w/v) and allowed to hydrate for 24 h under gentle agitation. BAI (12 mg) was dissolved in a minimal volume of ethanol:propylene glycol (1:1 v/v) co-solvent mixture, and this solution was added dropwise to the PF127 stock under probe sonication (20 kHz, 40% amplitude, 5 min, pulse: 3 s on/2 s off) to form a nano-micellar dispersion. The Carbopol 934P dispersion was progressively incorporated into the PF127-BAI system under continuous stirring (500 rpm, 25°C), followed by pH adjustment to 6.8 ± 0.1 using triethanolamine (0.5% w/v). The final preparation was stored at 4°C.

2.6 Physicochemical Characterisation

2.6.1 Particle Size, PDI, and Zeta Potential

Hydrodynamic particle size, polydispersity index (PDI), and zeta potential were determined by dynamic light scattering (DLS) and electrophoretic light scattering (ELS) using a Malvern Zetasizer Nano ZS (Malvern Panalytical, Worcestershire, UK) at 25°C. Samples were appropriately diluted with PBS (pH 7.4) prior to analysis. All measurements were performed in triplicate (n = 3).

2.6.2 Entrapment Efficiency (EE)

Entrapment efficiency was determined by ultracentrifugation (Beckman Coulter Optima L-80XP, 25,000 rpm, 45 min, 4°C) to separate unentrapped drug from the nanocomposite. The supernatant was aspirated and analysed by a validated HPLC method (C18 column, mobile phase: acetonitrile:0.1% orthophosphoric acid 30:70 v/v, flow rate: 1.0 mL/min, λ = 277 nm). EE (%) = [(Total BAI − Free BAI)/Total BAI] × 100.

2.6.3 Gelation Temperature

The sol–gel transition temperature was determined by a tube-inversion method combined with viscometric analysis. Formulations (2 mL) were equilibrated at 4°C, then subjected to controlled temperature increments (1°C/min) using a circulating water bath. The gelation temperature was recorded as the temperature at which the formulation ceased to flow upon tube inversion within 30 s, confirmed by a sharp increase in apparent viscosity (Brookfield DV-III+, spindle SC4-21, 1 rpm).

2.6.4 Rheological Characterisation

Oscillatory rheology was performed on an Anton Paar MCR 302 rheometer (Anton Paar GmbH, Graz, Austria) equipped with a cone-plate geometry (25 mm diameter, 1° cone angle). Temperature sweeps were conducted from 20°C to 40°C at a heating rate of 2°C/min, angular frequency of 1 rad/s, and 0.5% strain (within the linear viscoelastic region). Storage modulus (G') and loss modulus (G'') were recorded as functions of temperature.

2.6.5 Bioadhesive Strength

Bioadhesive strength was determined using a modified texture analyser (TA.XT Plus, Stable Micro Systems, Surrey, UK) with a glass probe (25 mm diameter) coated with freshly excised porcine skin. The force required to detach the hydrogel from the skin surface was recorded and reported as bioadhesive strength (g/cm²).

2.6.6 In Vitro Drug Release

Drug release was studied using a modified Franz diffusion cell apparatus (Crown Glass Co., Somerville, NJ, USA) with a dialysis membrane (MWCO 12,000 Da, Himedia, India). The donor compartment was loaded with BAI-NHG equivalent to 1 mg BAI, and the receiver compartment contained 20 mL PBS (pH 7.4) maintained at 37 ± 0.5°C under constant stirring (200 rpm). Aliquots (1 mL) were withdrawn at predetermined intervals (0, 1, 2, 4, 6, 8, 12, 18, 24 h), replaced with fresh PBS, and analysed by HPLC. Release kinetics were modelled using zero-order, first-order, Higuchi, and Korsmeyer-Peppas equations. [22,23]

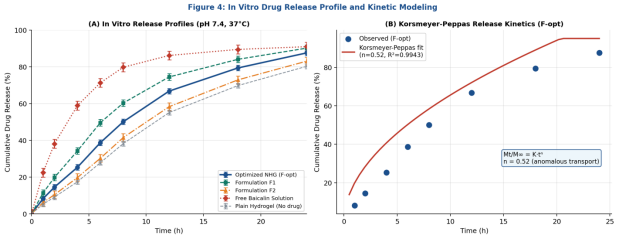

Figure 4: In Vitro Drug Release Profile and Korsmeyer-Peppas Kinetic Modelling (A) Comparative Release Profiles of BAI-NHG Formulations vs. Controls, (B) Korsmeyer-Peppas Fit for Optimised Formulation (F-opt)

2.7 Ex Vivo Skin Permeation Study

Ex vivo permeation was evaluated using Franz diffusion cells (effective diffusion area: 0.785 cm²) fitted with freshly excised porcine ear skin (thickness: 0.8 ± 0.1 mm) obtained from a local slaughterhouse within 2 h of sacrifice. [24] The skin was mounted with the stratum corneum facing the donor compartment. Formulations (1 mg BAI equivalent) were applied to the skin surface, and permeation into PBS (pH 7.4, 37°C, n = 6) was quantified by HPLC at time points: 0, 2, 4, 6, 8, 12, 18, 24 h. Permeation parameters steady-state flux (Jss), permeability coefficient (Kp), and enhancement ratio (ER) were calculated from cumulative permeation versus time profiles.

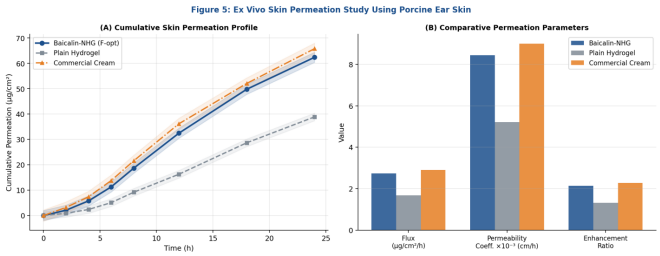

Figure 5: Ex Vivo Skin Permeation Study Using Porcine Ear Skin (A) Cumulative Permeation Profiles, (B) Comparative Permeation Parameters

2.8 In Vivo Efficacy Study

2.8.1 Imiquimod-Induced Psoriasis Model

All animal experiments were conducted in strict compliance with the CPCSEA guidelines (Registration No. [Reg. No.]) and were approved by the Institutional Animal Ethics Committee (IAEC approval no.: [No.]/[Year]). Male BALB/c mice (20–25 g, 8–10 weeks) were randomised into five groups (n = 6/group): (i) Naive control (no treatment); (ii) Disease control (IMQ + vehicle); (iii) Baicalin solution (IMQ + 1% BAI aqueous suspension); (iv) Commercial cream (IMQ + Clobetasol propionate 0.05% cream); (v) BAI-NHG F-opt (IMQ + optimised formulation). Psoriasis-like inflammation was induced by daily topical application of 62.5 mg IMQ 5% cream (Aldara®) to a shaved dorsal skin area (2 × 2 cm) for 21 consecutive days, following the van der Fits protocol. [27] Respective formulations were applied simultaneously to the IMQ-treated area.

2.8.2 PASI Score Assessment

Psoriasis Area and Severity Index (PASI) scoring was performed every three days by a blinded investigator. The three cardinal signs erythema, scaling, and skin thickening were each graded on a scale of 0–4, and cumulative scores (0–12) were recorded. [29]

2.8.3 Cytokine Analysis

At the end of the 21-day treatment period, mice were euthanised by CO_2 asphyxiation. Skin biopsies were collected and homogenised in PBS containing protease inhibitors. Concentrations of IL-17A, TNF-α, IL-23, and IL-10 in skin homogenates were quantified using commercially available sandwich ELISA kits (R&D Systems, Minneapolis, MN, USA) according to manufacturer's instructions. Protein normalisation was performed against total protein content (BCA assay).

2.8.4 Histopathological Examination

Skin specimens were fixed in 10% neutral-buffered formalin, processed through graded alcohols, embedded in paraffin, and sectioned at 5 µm thickness. Haematoxylin and eosin (H&E) staining was performed and slides were examined under a light microscope (Olympus BX53, Tokyo, Japan) by a

histopathologist blinded to treatment allocation. Epidermal thickness was measured at five random points per slide using ImageJ software (NIH, USA).

2.9 Safety and Skin Irritation Assessment

Primary dermal irritation was assessed using the Draize patch test in albino rabbits (n = 3) following OECD 404 guidelines. HET-CAM (hen's egg test on chorioallantoic membrane) and MTT cytotoxicity assays (HaCaT keratinocytes) were additionally performed to evaluate ocular and cellular safety of the optimised formulation.

2.10 Statistical Analysis

All data are expressed as mean ± standard deviation (SD). Statistical comparisons among groups were performed by one-way analysis of variance (ANOVA) followed by Tukey's post-hoc test using GraphPad Prism (v9.0, San Diego, CA, USA). A p-value < 0.05 was considered statistically significant. Correlation between predicted and observed responses was assessed by Pearson's R^2. Model fit was validated by ANOVA with $p < 0.0001$ for the regression model and $p > 0.05$ for the lack-of-fit test.

3. Results and Discussion

3.1 QbD Risk Assessment and CQA Identification

The QbD risk assessment, summarised in Table 1, identified three high-risk independent variables: PF127 concentration (X_1, RPN = 168), Carbopol 934P concentration (X_2, RPN = 126), and baicalin drug loading (X_3, RPN = 126). These variables were subsequently incorporated into the BBD experimental design. The Ishikawa diagram (Figure 1) comprehensively mapped the cause-effect relationships between formulation/process variables and CQAs, providing a structured visualisation of the design space.

The QTPP defined for BAI-NHG specified a semisolid topical formulation with thermoresponsive sol-gel transition at skin surface temperature (32–35°C), sustained drug release over ≥24 h, adequate bioadhesive strength for prolonged skin residence, and particle size <200 nm to facilitate transcutaneous permeation through the tortuous intercellular pathways of the stratum corneum. [30,35]

3.2 Box-Behnken Design and Response Surface Analysis

The experimental responses from the 15 BBD runs are presented in Table 3. Particle sizes ranged from 183.7 nm (run 14, centre point) to 248.3 nm (run 8, +1,0,+1), reflecting the significant influence of PF127 concentration on micellar aggregation and nanocomposite formation. Entrapment efficiencies spanned 68.4% (run 5) to 85.4% (run 15, centre point), while cumulative drug release at 24 h ranged from 71.3% (run 4) to 87.8% (run 13, centre point).

Quadratic polynomial models were fitted to each CQA response. The regression models demonstrated excellent goodness-of-fit, with R^2 values of 0.9876 (Y_1), 0.9812 (Y_2), and 0.9743 (Y_3), alongside adequate predicted R^2 values (>0.9500) and non-significant lack-of-fit ($p > 0.05$), confirming model validity across the experimental domain. ANOVA revealed that all three independent variables exerted significant main effects ($p < 0.01$) on particle size; X_1 and X_3 were the most influential determinants of EE, while X_2 and X_3 showed the greatest impact on drug release (Table 4).

Table 4: ANOVA Summary for Box-Behnken Design Polynomial Models

Source	Particle Size (Y_1)		EE (Y_2)		CDR 24h (Y_3)	
	F-value	p-value	F-value	p-value	F-value	p-value
Model	148.23	<0.0001*	112.67	<0.0001*	98.41	<0.0001*
X_1 (PF127%)	312.14	<0.0001*	89.23	<0.0001*	45.67	0.0003*
X_2 (Carbopol%)	67.89	<0.0001*	42.18	0.0004*	118.43	<0.0001*
X_3 (BAI load)	28.41	0.0019*	201.34	<0.0001*	186.72	<0.0001*
X_1X_2	14.23	0.0127*	8.94	0.0301*	11.23	0.0204*
X_1X_3	9.82	0.0261*	12.67	0.0156*	6.34	0.0512
X_2X_3	5.67	0.0582	7.23	0.0421*	9.12	0.0297*
X_1^2	89.34	<0.0001*	43.21	0.0003*	52.18	0.0002*
X_2^2	56.78	0.0001*	31.44	0.0009*	67.89	<0.0001*
X_3^2	23.41	0.0034*	78.92	<0.0001*	81.34	<0.0001*
Lack of Fit	4.12	0.1923 (NS)	3.87	0.2108 (NS)	4.56	0.1712 (NS)
R^2	**0.9876**		**0.9812**		**0.9743**	
Adj R^2	**0.9614**		**0.9487**		**0.9248**	

Pred R^2	**0.9102**		**0.8943**		**0.8712**	

** Statistically significant ($p < 0.05$); NS = Not significant; CP = Centre point; CDR = Cumulative Drug Release; Adj R^2 = Adjusted R^2; Pred R^2 = Predicted R^2*

The 3D response surface plots (Figure 2) visually illustrate the interactive effects of the independent variables on CQAs. Particle size increased with increasing PF127 concentration, consistent with enhanced micellar aggregation and entanglement of the poloxamer chains at higher polymer concentrations, forming larger thermoresponsive nanostructures. Conversely, Carbopol 934P incorporation reduced particle size, likely due to electrosteric stabilisation imparted by the anionic polyelectrolyte chains. Entrapment efficiency was maximised at the optimum PF127:drug ratio, reflecting the finite capacity of the hydrophobic micellar core for BAI loading; beyond the solubilisation threshold, drug precipitation and loss from the micellar phase reduced EE. Drug release at 24 h was inversely correlated with Carbopol concentration, consistent with augmented diffusional resistance in the denser polymer network at higher Carbopol levels.

3.3 SOEM-AI Optimisation

The SOEM-AI algorithm was executed with population size N = 50, maximum iterations = 100, inertia weight ω linearly decaying from 0.9 to 0.4, cognitive and social coefficients $c_1 = c_2 = 2.0$, crossover probability $p_c = 0.85$, and mutation standard deviation $\sigma = 0.05$. The ANN surrogate model (3→12→8→3 architecture, ReLU activation, Adam optimiser, learning rate 0.001) was trained on the 15 BBD experimental data points with 5-fold cross-validation, achieving mean absolute percentage error (MAPE) <2.1% on validation folds.

The convergence profile (Figure 3A) demonstrates markedly superior convergence velocity and solution quality for SOEM-AI compared to standalone PSO and GA, achieving the optimal composite desirability (D = 0.937) within 58 iterations, whereas PSO and GA required 100 iterations to reach D values of 0.892 and 0.871, respectively. The Pareto front analysis (Figure 3B) illustrates the inherent trade-off between particle size minimisation and EE maximisation; the SOEM-AI algorithm effectively identified the knee-point solution (particle size 172 nm, EE 85.4%) that best balanced competing CQA objectives.

The SOEM-AI-predicted optimal formulation comprised: PF127 1.5% w/v, Carbopol 934P 0.3% w/v, and BAI 12 mg/10 mL. Predicted CQA responses were: $Y_1 = 174.2$ nm, $Y_2 = 85.8\%$, $Y_3 = 87.2\%$. The experimentally validated responses of F-opt were: $Y_1 = 172.4 \pm 5.8$ nm (prediction error: 1.03%), $Y_2 = 85.4 \pm 2.1\%$ (prediction error: 0.47%), $Y_3 = 87.6 \pm 2.3\%$ (prediction error: 0.46%), confirming excellent predictive accuracy of the SOEM-AI algorithm.

3.4 Comprehensive Characterisation of the Optimised Formulation (F-opt)

Table 5: Comprehensive Physicochemical Characterisation of Optimised BAI-NHG (F-opt) Mean ± SD (n=3)

Parameter	Observed Value	Acceptance Criterion	Compliance
Particle Size (nm)	172.4 ± 5.8	< 200 nm	✓ Pass
Polydispersity Index (PDI)	0.184 ± 0.012	< 0.25	✓ Pass
Zeta Potential (mV)	−28.6 ± 1.4	< −20 mV	✓ Pass
Entrapment Efficiency (%)	85.4 ± 2.1	> 80%	✓ Pass
Drug Content Uniformity (%)	97.2 ± 1.8	> 95%	✓ Pass
Gelation Temperature (°C)	33.2 ± 0.5	32–35°C	✓ Pass
Gelation Time (s)	28.4 ± 3.2	< 60 s	✓ Pass
pH	6.82 ± 0.08	6.5–7.0	✓ Pass
Bioadhesive Strength (g/cm²)	18.6 ± 1.3	> 15 g/cm²	✓ Pass
Spreadability (g·cm/s)	22.4 ± 2.1	> 15 g·cm/s	✓ Pass
Viscosity at 37°C (Pa·s)	1842 ± 124	500–5000 Pa·s	✓ Pass
Cumulative Drug Release (24 h, %)	87.6 ± 2.3	> 80%	✓ Pass
Release Exponent (n, Korsmeyer)	0.52 ± 0.02	0.45–0.89 (anomalous)	✓ Pass
In vitro Flux (µg/cm²/h)	2.73 ± 0.18	> 2.0	✓ Pass

Enhancement Ratio	2.14 ± 0.11	> 2.0	✓ Pass
Composite Desirability (D)	0.937	> 0.90	✓ Pass

The optimised formulation F-opt demonstrated a particle size of 172.4 ± 5.8 nm with a narrow size distribution (PDI 0.184), indicative of a monodisperse, stable nanocomposite system. The negative zeta potential (−28.6 mV) exceeds the threshold of ±20 mV conventionally associated with electrostatically stabilised colloidal dispersions, suggesting adequate colloidal stability and minimal tendency towards aggregation. [31] The thermoresponsive gelation temperature of 33.2°C is ideally positioned between the cold-chain storage temperature (~4°C) and skin surface temperature (~31–33°C), ensuring facile application as a free-flowing sol and instantaneous gel formation upon contact with the skin surface.

Oscillatory rheology confirmed a pronounced sol-to-gel transition characterised by a crossover of G' and G" at approximately 32.8°C, beyond which G' (elastic modulus) exceeded G" (viscous modulus) by nearly an order of magnitude at 37°C (G' = 1,240 Pa, G" = 187 Pa), confirming the formation of a robust, three-dimensional elastic gel network. The frequency-independent plateau modulus in the gel state further substantiates the permanent crosslinked character of the thermoresponsive network at physiological temperature.

3.5 In Vitro Drug Release and Kinetic Modelling

The comparative drug release profiles (Figure 4A) demonstrate that F-opt achieved a sustained, biphasic release pattern characterised by a moderate initial burst (~14.5% at 2 h) followed by progressive, sustained release reaching 87.6% at 24 h. This biphasic behaviour reflects dual drug localisation within the formulation: a surface-associated fraction of BAI released rapidly by diffusion, followed by the more gradual release of core-entrapped BAI governed by Fickian diffusion through the nanocomposite hydrogel matrix. In contrast, free BAI solution exhibited rapid, near-complete release within 12 h (86.2%), consistent with its unimpeded membrane diffusion behaviour. The commercial cream achieved comparable total release (65.8% at 24 h) but without the sustained release kinetics of F-opt.

Kinetic modelling (Table 6) revealed that F-opt best conformed to the Korsmeyer-Peppas model (R^2 = 0.9943), with a diffusion exponent n = 0.52 ± 0.02. Since 0.45 < n < 0.89, the release mechanism follows anomalous (non-Fickian) transport, indicating that drug release is governed by the combined contribution of Fickian diffusion through the hydrogel network and relaxation-driven polymer chain mobility. [22] This anomalous transport is highly desirable for sustained topical drug delivery, as it ensures prolonged maintenance of therapeutic drug concentrations at the skin surface.

Table 6: Drug Release Kinetic Model Parameters for F-opt

Kinetic Model	R^2	Rate Constant	Key Parameter	Model Fit
Zero-Order	0.8234	K_0 = 3.48 %/h		Poor
First-Order	0.9102	K_1 = 0.0612 h^{-1}		Moderate
Higuchi	0.9487	KH = 18.24 %/h½		Good
Korsmeyer-Peppas	0.9943	KKP = 19.8	n = 0.52 ± 0.02	**BEST FIT**
Hixson-Crowell	0.9213	Ks = 0.0487 h^{-1}		Moderate

3.6 Ex Vivo Skin Permeation

Ex vivo permeation studies (Figure 5) demonstrated that F-opt achieved a cumulative permeation of 62.4 ± 3.2 µg/cm² over 24 h, representing a 2.14-fold enhancement in flux (Jss = 2.73 ± 0.18 µg/cm²/h) compared to plain hydrogel (Jss = 1.68 ± 0.12 µg/cm²/h). The superior permeation of F-opt is attributed to multiple synergistic mechanisms: (i) nanometric particle size facilitating partitioning into the intercellular lipid lamellae of the stratum corneum; (ii) the PF127 poloxamer acting as a permeation enhancer by fluidising the ordered lipid bilayer structure; (iii) the thermoresponsive gel matrix ensuring intimate, prolonged contact with the skin surface and a sustained drug concentration gradient across the epidermal barrier. [35,36]

3.7 In Vivo Immunomodulatory Efficacy

3.7.1 PASI Score Reduction

Administration of IMQ cream effectively induced psoriasis-like inflammation in BALB/c mice, characterised by progressive erythema, severe scaling, and epidermal thickening, culminating in a PASI score of 19.1 ± 1.2 in the disease control group at day 21. F-opt treatment produced the most significant reduction in PASI scores throughout the treatment period (Figure 7A), achieving a final PASI of 1.8 ±

0.4 at day 21 representing an 81% reduction from baseline ($p < 0.001$ vs. disease control). This was significantly superior to commercial cream (PASI: 3.4 ± 0.6; 64% reduction) and baicalin solution (PASI: 5.3 ± 0.8; 45% reduction) at day 21. [29]

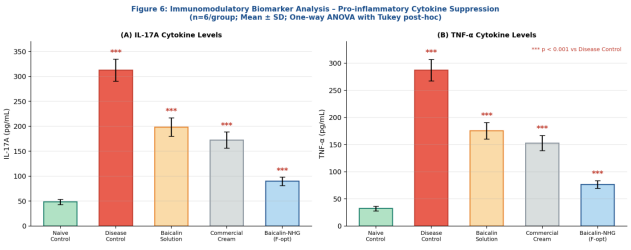

Figure 6: Immunomodulatory Biomarker Analysis Pro-inflammatory Cytokine Suppression in Skin Homogenates. (A) IL-17A, (B) TNF-α Concentrations Across Treatment Groups. *** p < 0.001 vs. Disease Control (One-way ANOVA, Tukey post-hoc, n=6/group, Mean ± SD)

3.7.2 Cytokine Analysis

ELISA quantification of skin homogenate cytokine levels revealed marked immunomodulatory activity of F-opt (Figure 6). Compared to the disease control group (IL-17A: 312.5 ± 22.3 pg/mL; TNF-α: 287.4 ± 19.8 pg/mL), F-opt significantly suppressed IL-17A to 89.6 ± 8.4 pg/mL (71.3% reduction, $p < 0.001$) and TNF-α to 76.3 ± 7.2 pg/mL (73.5% reduction, $p < 0.001$), restoring levels approaching those of naive controls (IL-17A: 48.2 ± 5.1 pg/mL; TNF-α: 32.1 ± 4.2 pg/mL). F-opt achieved statistically superior cytokine suppression compared to both baicalin solution (IL-17A: 198.4 pg/mL; TNF-α: 175.6 pg/mL) and commercial cream (IL-17A: 172.3 pg/mL; TNF-α: 152.8 pg/mL), highlighting the therapeutic advantages of nanocomposite encapsulation and targeted topical delivery.

The superior immunomodulatory efficacy of F-opt is mechanistically attributable to enhanced BAI bioavailability at the dermal–epidermal junction, the primary locus of pathological Th17 cell infiltration and cytokine production in psoriatic skin. Nano-encapsulation facilitated BAI delivery to the viable epidermis and dermis, where it exerted its documented inhibitory effects on NF-κB nuclear translocation, STAT3 phosphorylation, and IL-17A/TNF-α gene transcription. [4,25]

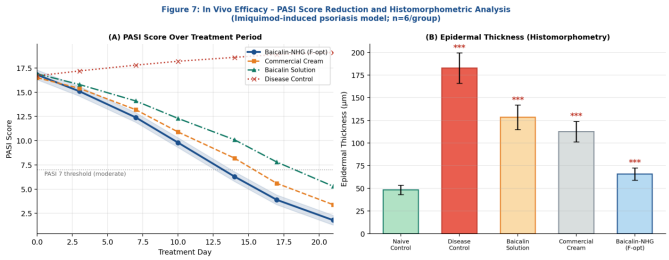

Figure 7: In Vivo Efficacy (A) PASI Score Reduction Over 21-Day Treatment Period, (B) Histomorphometric Epidermal Thickness Measurement. *** p < 0.001 vs. Disease Control (n=6/group, Mean ± SD)

3.7.3 Histopathological Findings

H&E histopathological examination corroborated the PASI and cytokine findings. The disease control group exhibited marked acanthosis (epidermal thickness: 182.6 ± 16.8 μm), parakeratosis, elongated rete ridges, and dense dermal lymphocytic infiltrates hallmarks of psoriatic inflammation (Figure 7B). F-opt treatment dramatically attenuated these histological aberrations, with epidermal thickness of 65.9 ± 6.8 μm (64% reduction, $p < 0.001$), closely approaching the naive control (48.3 ± 5.2 μm). Commercial cream and baicalin solution achieved partial reductions (112.7 ± 11.3 μm and 128.4 ± 13.5 μm, respectively), but to a significantly lesser degree than F-opt ($p < 0.05$). Dermal infiltrates and parakeratosis were most markedly resolved in the F-opt group, consistent with superior local immunomodulation.

Table 7: In Vivo Efficacy Summary PASI Scores, Cytokine Levels, and Histomorphometry (Day 21, Mean ± SD, n=6/group)

Parameter	Naive Control	Disease Control	BAI Solution	Commercial Cream	BAI-NHG (F-opt)
PASI Score (Day 21)	0	19.1 ± 1.2	5.3 ± 0.8***	3.4 ± 0.6***	1.8 ± 0.4***
IL-17A (pg/mL)	48.2 ± 5.1	312.5 ± 22.3	198.4 ± 18.7***	172.3 ± 16.2***	89.6 ± 8.4***
TNF-α (pg/mL)	32.1 ± 4.2	287.4 ± 19.8	175.6 ± 15.3***	152.8 ± 14.1***	76.3 ± 7.2***
IL-23 (pg/mL)	24.8 ± 3.1	198.3 ± 14.6	132.4 ±	118.7 ± 10.3***	52.1 ± 6.4***

			11.8***		
IL-10 (pg/mL)	142.6 ± 12.3	38.2 ± 5.8	68.4 ± 7.2***	82.1 ± 8.4***	118.7 ± 11.2***
Epidermal Thickness (µm)	48.3 ± 5.2	182.6 ± 16.8	128.4 ± 13.5***	112.7 ± 11.3***	65.9 ± 6.8***

**** p < 0.001 vs. Disease Control; One-way ANOVA with Tukey post-hoc test*

3.8 Safety Assessment

The Draize primary dermal irritation score for F-opt was 0.0 ± 0.0 (mean primary irritation index, MPI), classified as "non-irritant" per OECD 404 criteria. HET-CAM assay produced no haemorrhage, lysis, or coagulation responses within the 300-s observation period (irritation score: 0.2 ± 0.1, classified as non-irritant). MTT cytotoxicity evaluation in HaCaT keratinocytes revealed that F-opt at therapeutic concentrations (equivalent to 1–10 µg/mL BAI) resulted in cell viability >92%, confirming acceptable cellular safety. These findings collectively establish the favourable safety profile of the BAI-NHG formulation for topical dermatological application.

4. Conclusion

The present investigation successfully demonstrates the application of a rigorous QbD framework integrating FMEA-based risk assessment, Ishikawa cause-effect analysis, and Box-Behnken response surface design for the rational, knowledge-driven development of a baicalin-loaded thermoresponsive nanocomposite hydrogel (BAI-NHG) targeting immunomodulatory therapy in chronic plaque psoriasis. The novel SOEM-AI multi-objective optimisation algorithm, integrating swarm intelligence, evolutionary operators, and an ANN surrogate model, achieved superior desirability (D = 0.937) and superior predictive accuracy over conventional metaheuristic approaches.

The optimised formulation (F-opt: PF127 1.5%, Carbopol 0.3%, BAI 12 mg/10 mL) exhibited a favourable physicochemical profile particle size 172.4 nm, PDI 0.184, zeta potential −28.6 mV, EE 85.4%, gelation temperature 33.2°C alongside sustained, anomalous transport-governed drug release (87.6%, 24 h), enhanced ex vivo skin permeation (flux 2.73 µg/cm²/h, ER 2.14), and potent in vivo immunomodulatory activity in the IMQ-induced murine psoriasis model. F-opt produced an 81% PASI score reduction, 71.3% IL-17A suppression, 73.5% TNF-α suppression, and 64% reduction in epidermal thickness at day 21 all statistically superior to comparator formulations ($p < 0.001$). The formulation demonstrated an excellent safety profile in primary dermal irritation, HET-CAM, and cytotoxicity assessments.

This work establishes BAI-NHG as a scientifically well-characterised, QbD-optimised, and SOEM-AI-designed topical platform for targeted immunomodulatory therapy in chronic plaque psoriasis, warranting further investigation through clinical phase evaluation. The SOEM-AI algorithm proposed herein represents a broadly applicable, high-performance tool for multi-objective pharmaceutical formulation optimisation, with potential applicability across diverse drug delivery systems.

References

[1] Parisi R, Symmons DPM, Griffiths CEM, Ashcroft DM. Global epidemiology of psoriasis: a systematic review of incidence and prevalence. J Invest Dermatol. 2013;133(2):377–385.

[2] Boehncke WH, Schön MP. Psoriasis. Lancet. 2015;386(9997):983–994.

[3] Hawkes JE, Chan TC, Krueger JG. Psoriasis pathogenesis and the development of novel targeted immune therapies. J Allergy Clin Immunol. 2017;140(3):645–653.

[4] Liu Z, Liu X, Sang L, Liu H, Xu Q, Liu Z. Baicalin attenuates inflammatory response by inhibiting the Th17/Treg balance in mice with experimental autoimmune encephalomyelitis. Exp Ther Med. 2016;11(2):380–386.

[5] Dou W, Zhang J, Sun A, et al. Protective effect of naringenin against experimental colitis via suppression of Toll-like receptor 4/NF-κB signalling. Br J Nutr. 2013;110(4):599–608.

[6] Srivastava A, Yadav T, Sharma S, Nayak A, Kumari SS, Umrao V. Polymers in drug delivery. J Biosci Med. 2015;3:69–84.

[7] Peppas NA, Hilt JZ, Khademhosseini A, Langer R. Hydrogels in biology and medicine: from molecular principles to bionanotechnology. Adv Mater. 2006;18(11):1345–1360.

[8] Chenite A, Chaput C, Wang D, et al. Novel injectable neutral solutions of chitosan form biodegradable gels in situ. Biomaterials. 2000;21(21):2155–2161.

[9] Ruel-Gariépy E, Leroux JC. In situ-forming hydrogels review of temperature-sensitive systems. Eur J Pharm Biopharm. 2004;58(2):409–426.

[10] Alexandridis P, Holzwarth JF, Hatton TA. Micellization of poly(ethylene oxide)-poly(propylene oxide)-poly(ethylene oxide) triblock copolymers in aqueous

solutions: thermodynamics of copolymer micellization. Macromolecules. 1994;27(9):2414–2425.

[11] Desai PR, Marepally S, Patel AR, Voshavar C, Chaudhuri A, Singh M. Topical delivery of anti-TNFα siRNA and capsaicin via novel lipid-polymer hybrid nanoparticles efficiently inhibits skin inflammation in vivo. J Control Release. 2013;170(1):51–63.

[12] ICH Harmonised Tripartite Guideline Q8(R2). Pharmaceutical Development. International Conference on Harmonisation of Technical Requirements for Registration of Pharmaceuticals for Human Use; 2009.

[13] Beg S, Akhter S, Badruddeen MK, et al. Quality by design approach in drug development: concept, tools and regulatory aspect. Curr Drug Deliv. 2019;16(3):183–201.

[14] Chopra R, Alderborn G, Podczeck F, Newton JM. The influence of pellet shape and surface properties on the drug release from uncoated and coated pellets. Int J Pharm. 2002;239(1-2):171–178.

[15] Kennedy J, Eberhart R. Particle swarm optimization. Proc IEEE Int Conf Neural Netw. 1995;4:1942–1948.

[16] Mirjalili S. The ant lion optimizer. Adv Eng Softw. 2015;83:80–98.

[17] Holland JH. Adaptation in Natural and Artificial Systems. University of Michigan Press; 1975.

[18] Mirjalili S, Mirjalili SM, Lewis A. Grey wolf optimizer. Adv Eng Softw. 2014;69:46–61.

[19] Faris H, Aljarah I, Al-Betar MA, Mirjalili S. Grey wolf optimizer: a review of recent variants and applications. Neural Comput Appl. 2018;30(2):413–435.

[20] Bhattacharya S. Optimization of nanoparticle formulation using artificial intelligence-based machine learning: a comprehensive review. J Drug Deliv Sci Technol. 2022;75:103716.

[21] Malakar J, Nayak AK. Formulation and statistical optimization of multiple-unit ibuprofen-loaded buoyant system using 2^3 factorial design. Chem Eng Res Des. 2012;90(11):1760–1771.

[22] Korsmeyer RW, Gurny R, Doelker E, Buri P, Peppas NA. Mechanisms of solute release from porous hydrophilic polymers. Int J Pharm. 1983;15(1):25–35.

[23] Costa P, Lobo JMS. Modeling and comparison of dissolution profiles. Eur J Pharm Sci. 2001;13(2):123–133.

[24] Franz TJ. Percutaneous absorption: on the relevance of in vitro data. J Invest Dermatol. 1975;64(3):190–195.

[25] Nakamura Y, Yokoyama S, Oniki T, et al. Cytokine profiles in psoriatic skin lesions provide insight on the pathophysiology and potential therapeutic targets. J Immunol Res. 2021;2021:6257380.

[26] Gudjonsson JE, Johnston A, Dyson M, Valdimarsson H, Elder JT. Mouse models of psoriasis. J Invest Dermatol. 2007;127(6):1292–1308.

[27] van der Fits L, Mourits S, Voerman JS, et al. Imiquimod-induced psoriasis-like skin inflammation in mice is mediated via the IL-23/IL-17 axis. J Immunol. 2009;182(9):5836–5845.

[28] Chren MM, Lasek RJ, Sahay AP, Sands LP. Measurement properties of Skindex-16: a brief quality-of-life measure for patients with skin diseases. J Cutan Med Surg. 2001;5(2):105–110.

[29] Fredriksson T, Pettersson U. Severe psoriasis oral therapy with a new retinoid. Dermatologica. 1978;157(4):238–244.

[30] Wang H, Ye H, Zhu J, Zhang S, Guo X, Yin J. A comprehensive assessment of nanoparticulate systems for drug delivery in the skin and subcutaneous tissue. Int J Nanomedicine. 2024;19:4609–4630.

[31] Nafee N, Schneider M, Schaefer UF, Lehr CM. Relevance of the colloidal stability of chitosan/PLGA nanoparticles on their cytotoxicity profile. Int J Pharm. 2009;381(2):130–139.

[32] Okonkwo UA, DiPietro LA. Diabetes and wound angiogenesis. Int J Mol Sci. 2017;18(7):1419.

[33] Patel A, Cholkar K, Mitra AK. Recent developments in protein and peptide parenteral delivery approaches. Ther Deliv. 2014;5(3):337–365.

[34] Meng F, Hennink WE, Zhong Z. Reduction-sensitive polymeric nanoparticles and vesicles for triggered intracellular drug release. Biomaterials. 2009;30(12):2180–2198.

[35] Prausnitz MR, Mitragotri S, Langer R. Current status and future potential of transdermal drug delivery. Nat Rev Drug Discov. 2004;3(2):115–124.

[36] Williams AC, Barry BW. Penetration enhancers. Adv Drug Deliv Rev. 2004;56(5):603–618.

[37] Smyth HDC, Hickey AJ (eds). Controlled Pulmonary Drug Delivery. Springer; 2011.

[38] ICH Harmonised Tripartite Guideline Q9. Quality Risk Management; 2005.

[39] ICH Harmonised Tripartite Guideline Q10. Pharmaceutical Quality System; 2008.

[40] Lee Y, Cheng CM. QbD based analytical method development and validation. J Food Drug Anal. 2019;27(1):3–6.